Efficient Invariant-Manifold, Low-Thrust Planar Trajectories to the Moon

G. Mingotti[a,1,*], F. Topputo[b,1], F. Bernelli-Zazzera[b,2]

[a] *Institut für Industriemathematik, Universität Paderborn, Warburger Str. 100, 33098 Paderborn, Germany*
[b] *Dipartimento di Ingegneria Aerospaziale, Politecnico di Milano, Via La Masa 34, 20156 Milano, Italy*

Abstract

Two-impulse trajectories as well as mixed invariant-manifold, low-thrust efficient transfers to the Moon are discussed. Exterior trajectories executing ballistic lunar capture are formalized through the definition of special attainable sets. The coupled restricted three-body problems approximation is used to design appropriate first guesses for the subsequent optimization. The introduction of the Moon-perturbed Sun–Earth restricted four-body problem allows us to formalize the idea of ballistic escape from the Earth, and to take explicitly advantage of lunar fly-by. Accurate first guess solutions are optimized, through a direct method approach and multiple shooting technique.

Keywords: Nonlinear astrodynamics, N-body problem, Low-energy trajectories, Dynamical system theory, Low-thrust propulsion, Optimal control theory.

1. Introduction

Low energy transfers to the Moon are being studied since the rescue of the Japanese spacecraft Hiten in 1991.[1] In essence, a low energy lunar transfer reduces the hyperbolic excess velocity upon Moon arrival, typical of a patched-conics approach. This process is called ballistic capture, and relies on a better exploitation of the gravitational nature ruling the transfer problem instead of the classic Keplerian decomposition of the solar system. The reduced speed relative to the Moon sets the trajectory to low energy levels, which in turn imply a reduced propellant mass needed to stabilize the spacecraft around the Moon.

It is known that the dynamical mechanism governing a class of exterior low energy transfers to the Moon is related to the structure of the invariant manifolds associated with the Lyapunov orbits about the collinear libration points.[2] In particular, a systematic method for the construction of low energy transfers using the knowledge of the phase space

*Corresponding author
Email addresses: giorgio.mingotti@mail.polimi.it (G. Mingotti), topputo@aero.polimi.it (F. Topputo), bernelli@aero.polimi.it (F. Bernelli-Zazzera)
[1] Postdoctoral Fellow
[2] Full Professor

of the Sun–Earth and Earth–Moon systems is given in the works of the *Caltech* and the *Barcelona* groups.[3,4,5]

Previous works have faced the combination of n-body dynamics with low-thrust propulsion. An interior ballistic capture state using low-thrust propulsion was found in.[6] This approach paved the way for the design of the trajectory for ESA's SMART-1 mission.[7] Earth–Venus transfers have been obtained in[8] by combining invariant manifold dynamics and low-thrust, with set oriented methods. Moreover, there are also some examples of the integration of dynamical system theory and optimal control problems for the design of efficient low-energy, low-thrust transfers to the halo orbits.[9,10]

In this paper, both efficient two-impulse transfers and the low-thrust version of the transfers described in[3] are presented, all of them starting from the same LEO with an impulsive maneuver given by the launcher. It is in fact possible to further reduce the propellant necessary to send a spacecraft to the Moon by exploiting both the simultaneous gravitational attractions of the Sun, the Earth, and the Moon, and the high specific impulse provided by the low-thrust engines (above 1000 seconds). Nevertheless, including the low-thrust is not trivial, and asks for a number of issues to face. It is of great importance, for instance, overcoming the loss of Jacobi integral, finding subsets of the phase space that lead to low-thrust ballistic capture (playing the separatrix-like role of the stable manifold associated with L_2 Lyapunov orbit of the Earth–Moon system), and summarizing, using as few parameters as possible, all the reachable orbits that it is possible to target with the finite thrust magnitude available, like low lunar orbits (LLOs).

This paper follows a previous study on transfers from the Earth to the Moon proposed by the same authors.[11] Several improvements have been made since that study, in terms of mathematical formalism, new applicative scenarios and results obtained.

- A new dynamical model is described, the Moon-perturbed Sun-Earth restricted four-body problem: first guess solution which explicitly exploit the lunar flyby can be defined.
- The idea of attainable sets is introduced as a unique formal approach to describe both ballistic and low-thrust arcs.
- Two different types of mission are investigated, one involving a ballistic capture at the Moon, the other concerning a low-thrust insertion.
- The results obtained for both scenarios are presented with respect to more accurate and fair evaluation parameters, and they outperform our previous study in terms of propellant mass consumption and flight time.

The purpose of this work is therefore to formulate a systematic approach for the design of efficient pure low-energy as well as mixed invariant-manifold, low-thrust transfers to low orbits around the Moon. A comparison between the trajectories computed and some solutions found in literature is presented.

The remainder of the paper is organized as follows: first a brief recall of the dynamics involved in the problem is given. Then a description of the trajectory design strategy to

low Moon orbits and the introduction of special *attainable sets* are given. Finally, the optimization problem is formulated and later the optimal solutions are discussed.

2. Design Strategy

With the *coupled restricted three-body problems approximation*, the four-body dynamics, characterizing the low energy lunar transfers, is decomposed into two restricted three-body problems (RTBPs), and the invariant manifolds of the Lyapunov orbits are computed. It is possible to show that, with a suitably chosen Poincaré section, the trajectory design is restricted to the selection of a single point on this section.[3] Flown backward, this initial condition gives rise to a trajectory close to the stable and unstable manifolds of the L_j, for $j = 1, 2$, Lyapunov orbits of the Sun–Earth system; integrated forward, a transit, lunar ballistic capture orbit (i.e., an orbit contained inside the stable manifold tube-like structure of the L_2 Lyapunov orbit of the Earth–Moon system) is achieved. A small Δv maneuver is eventually needed at this patching point, in order to match the energies of the two stages. With this approach, it is possible to find efficient Earth–Moon transfers like the ones described in.[1]

The transfers studied in this work are defined as follows. The spacecraft is assumed to be initially on a circular parking orbit around the Earth at a height $h_E = 167\,\mathrm{km}$; then an impulsive maneuver, Δv_E, carried out by the launch vehicle, places the spacecraft on a translunar trajectory, performing a translunar insertion (TLI). Two different typologies of mission are investigated, according to the propulsion adopted: (i) low-energy, two-impulse transfers to LLOs: after the insertion, the spacecraft flies ballistically under the four-body dynamics and reaches the Moon, where a second impulsive maneuver inserts it on a stable low altitude orbit; (ii) low-energy, low-thrust transfers to LLOs: after the launch, the spacecraft can only rely on its low-thrust propulsion to reach a stable low-altitude orbit around the Moon.

As for these transfers, the final orbit has moderate eccentricity, e, and periapsis/apoapsis, r_p/r_a, prescribed by the mission requirements. The transfer terminates when the spacecraft is at the periapsis of the final orbit around the Moon. While both e and r_p/r_a are assumed to be given, the orientation, i.e., the argument of periapsis, ω, of the final orbit around the Moon is not fixed.

In general, the two transfer families are achieved by optimizing, in a four-body scenario, a first guess derived in the coupled three-body problems approximation. From the prospective of this model, the transfer trajectory is conceived as made up by two distinct portions: the first, called Earth escape stage, is built in the Sun–Earth model, SE, whereas the second, called Moon capture stage, is defined in the Earth–Moon model, EM.

2.1. The Planar Circular Restricted Three-Body Problem

The motion of the spacecraft, m_3, is studied in the gravitational field generated by the mutual circular motion of two primaries of masses m_1, m_2, respectively, about their

common center of mass (see Fig. 3(a)). It is assumed that m_3 moves in the same plane of m_1, m_2 under the following equations:[12]

$$\ddot{x} - 2\dot{y} = \frac{\partial \Omega}{\partial x}, \qquad \ddot{y} + 2\dot{x} = \frac{\partial \Omega}{\partial y}, \tag{1}$$

where the auxiliary function is

$$\Omega(x, y, \mu) = \frac{1}{2}(x^2 + y^2) + \frac{1-\mu}{r_1} + \frac{\mu}{r_2} + \frac{1}{2}\mu(1-\mu), \tag{2}$$

and $\mu = m_2/(m_1 + m_2)$ is the mass parameter of the three-body problem. Eqs. (1) are written in a barycentric rotating frame with nondimensional units: the angular velocity of m_1, m_2, their distance, and the sum of their masses are all set to the unit value. It is easy to verify that the primary of mass $1 - \mu$, is located at $(-\mu, 0)$, whereas the smaller primary μ, is located at $(1 - \mu, 0)$; thus, the distances between m_3 and the primaries are:

$$r_1^2 = (x + \mu)^2 + y^2, \qquad r_2^2 = (x + \mu - 1)^2 + y^2. \tag{3}$$

For fixed μ, the Jacobi integral reads

$$J(x, y, \dot{x}, \dot{y}) = 2\Omega(x, y, \mu) - (\dot{x}^2 + \dot{y}^2), \tag{4}$$

and, for a given energy C, it defines a three-dimensional manifold

$$F(C) = \{(x, y, \dot{x}, \dot{y}) \in \mathcal{R}^4 | J(x, y, \dot{x}, \dot{y}) - C = 0\}, \tag{5}$$

foliating the four-dimensional phase space. The projection of $F(C)$ on the configuration space (x, y) defines the Hill's curves bounding the allowed and forbidden regions associated with prescribed values of C. The vector field defined by Eqs. (1) has five well-known equilibrium points, known as the Lagrange points, labeled L_j, $j = 1, \ldots, 5$. This study deals with the portion of the phase space surrounding the two collinear points L_1 and L_2. In a linear analysis, these two points behave like the product *saddle* $\times$ *center*. Thus, there exists a family of retrograde Lyapunov orbits and two-dimensional stable and unstable manifolds emanating from them.[13,14]

The system governed by Eqs. (1) is used alternatively to describe the motion of the spacecraft either in the Sun–Earth (SE) or in the Earth–Moon (EM) system. The mass-parameter value assumed for these models are $\mu_{SE} = 3.0034 \times 10^{-6}$ and $\mu_{EM} = 1.2150 \times 10^{-2}$, respectively.

As for the SE model, the generic periodic orbit about L_j, $j = 1, 2$, is referred to as γ_j, whereas its stable and unstable manifolds are labeled $W^s(\gamma_j)$, $W^u(\gamma_j)$. Dealing with the EM model, the generic periodic orbit about L_j, $j = 1, 2$, is called λ_j, while its stable and unstable manifolds are named $W^s(\lambda_j)$, $W^u(\lambda_j)$.

3. Earth Escape Stage

If a value of Jacobi constant in the SE model, C_{SE}, is suitably chosen, there exists a unique Lyapunov orbit about both L_1 and L_2, labeled γ_1 and γ_2, respectively. Assuming the energy values $C_{SE} \ll C_{2-SE}$ (where C_{2-SE} is the Jacobi constant of L_2 in the

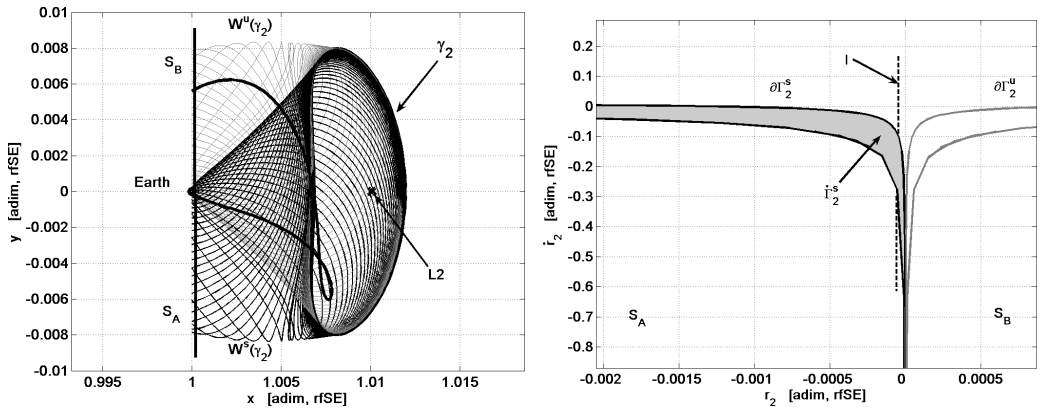

(a) $W^s(\gamma_2)$ and $W^u(\gamma_2)$.

(b) $\partial\Gamma_2^s$, $\dot{\Gamma}_2^s$ and $\partial\Gamma_2^u$ sets.

Figure 1: Stable and unstable manifolds $W^s(\gamma_2)$, $W^u(\gamma_2)$ associated with the L_2 Lyapunov orbit γ_2, and their section curves $\partial\Gamma_2^s$, $\partial\Gamma_2^u$, respectively. In Figure 1(a), the bold line stands for a sample Earth escape trajectory. In Figure 1(b), the set $\dot{\Gamma}_2^s$ (grey) is made up by the points of S_A that lie inside $\partial\Gamma_2^s$, whereas the line l (dashed) is the locus of points being at $h_E = 167\,\text{km}$ altitude above the Earth surface.

SE model) such that both γ_1 and γ_2 exist, the Hill's regions are opened at both L_1 and L_2. Without any loss of generality, the Earth escape stage is constructed considering the dynamics around L_2; using L_1 instead of L_2 is straightforward. The stable and unstable manifolds associated with γ_2, $W^s(\gamma_2)$ and $W^u(\gamma_2)$, are computed starting from the Lyapunov orbit until a certain surface of section is reached.

Aiming at exploiting the structure of both $W^s(\gamma_2)$ and $W^u(\gamma_2)$, two surfaces of section are introduced to study their cuts at different stages. Section S_A, making an angle φ_A (clockwise) with the x-axis and passing through the Earth, is considered to cut $W^s(\gamma_2)$, whereas section S_B, inclined by φ_B (counterclockwise) on the x-axis and passing through the Earth, is assumed for $W^u(\gamma_2)$ (see Fig. 1(a) for the two manifolds topology, and see Fig. 2(a) for the two angles). The corresponding section curves, $\partial\Gamma_2^s$, $\partial\Gamma_2^u$, represented on the $(r_2, \dot{r}_2)$-plane, are diffeomorphic to circles (see Fig. 1(b), $\partial\Gamma_2^s$, $\partial\Gamma_2^u$ are plotted on the $(r_2, \dot{r}_2)$-plane as $r_2 = y$, $\dot{r}_2 = \dot{y}$ for $x = 1 - \mu$, $\varphi_A = \varphi_B = \pi/2$).

Both Poincaré sections represent two-dimensional maps for the flow of the RTBP. Indeed, any point on these sections uniquely defines an orbit. This property holds as both $F(C_{SE})$ and $S_{A,B}$ lower the dimension of the phase space to two. By definition, points on $\partial\Gamma_2^s$ generate orbits that asymptotically approach γ_2 in forward time. Points inside Γ_2^s give rise to transit orbits that pass from the Earth region to the exterior region, whereas points outside Γ_2^s correspond to nontransit orbits (the manifolds act as separatrices for the states of motion[13,14]).

Candidate trajectories for Earth–Moon transfers are nontransit orbits close to both $W^s(\gamma_2)$ and $W^u(\gamma_2)$. This property is wanted since the existence of $W^s(\gamma_2)$ and $W^u(\gamma_2)$ has to be exploited, although the transfer orbit does not exactly lie on any invariant subset. Let $\dot{\Gamma}_2^s$ be the set of points in the $(r_2, \dot{r}_2)$-plane that are enclosed by $\partial\Gamma_2^s$, and $\bar{\Gamma}_2^s$ the closed

set made up of $\partial\,\Gamma_2^s \cup \dot{\Gamma}_2^s$ (see Fig. 1(b)). Points on $\bar{\Gamma}_2^s$ have to be avoided as they lead to either transit or asymptotic orbits. On the contrary, all the points that lie on

$$l = \{(r_2, \dot{r}_2) \in S_A,\, (r_2, \dot{r}_2) \notin \bar{\Gamma}_2^s | r_2 = R_E + h_E\} \tag{6}$$

are translunar candidate orbits as they intersect the initial parking orbit (R_E is the radius of the Earth). This intersection occurs in the configuration space only, as the initial parking orbit and the translunar trajectory have two different energy levels.

The pair $\{C_{SE},\, \varphi_A\}$ uniquely defines the curve $\partial\,\Gamma_2^s$ on S_A: C_{SE} stands for the orbit γ_2, whereas φ_A defines the surface of section S_A to cut the first intersection of $W^s(\gamma_2)$. Thus, $\{C_{SE},\, \varphi_A\}$ are used to define the first guess Earth escape stage. In order to obtain efficient transfer trajectories, the lowest possible initial instantaneous maneuver, Δv_E, is searched. It is necessary to define its components: a first contribution to the Δv_E amount is related to the radial term Δv_r, while the second tangential contribution Δv_t is needed to fill the gap ΔC between the energy of the initial parking orbit, C_E, and C_{SE} (i.e., $\Delta C = C_E - C_{SE}$). It is possible to show that $\Delta v(\Delta C, \varphi_A) = \Delta v_t(\Delta C) + \Delta v_r(\varphi_A)$, and it is even possible to lower Δv_r to zero by properly tuning φ_A. This approach leads to initial tangential maneuvers (the initial Δv_E is aligned with the velocity of the circular parking orbit around the Earth). The search is therefore restricted to the point $P \in S_A$ defined by $P = l \cap l'$, where l' is the set of points having zero radial velocity with respect to the Earth

$$l' = \{(r_2, \dot{r}_2) \in S_A,\, (r_2, \dot{r_2}) \notin \bar{\Gamma}_2^s | \dot{r}_2 = 0\}. \tag{7}$$

Point P does not exactly lie on the stable manifold (but outside), and can be found sufficiently close to $W^s(\gamma_2)$ by suitably tuning φ_A (see Fig. 2(b)). In practice, since at this stage a first guess solution is constructed to be later optimized, orbits sufficiently close to P can also be considered. In particular, points $P' \in S_A$ such that $\|P' - P\| \leq \varepsilon$ are also taken into account, where ε is a certain prescribed distance.

A number of P' points can be generated by tuning the angle φ_A. These points, flown forward, generate orbits that are close to $W^s(\gamma_2)$ until the region about γ_2 is reached. From this point on, the orbits get close to $W^u(\gamma_2)$, and their intersection with S_B is studied. The set labeled $\mathcal{E}_{SE}$, $\mathcal{E}_{SE} \in S_B$, stands for the set of orbits close to $W^u(\gamma_2)$ whose pre-image $\mathcal{E}_{SE}^{-1}$, $\mathcal{E}_{SE}^{-1} \in S_A$, is made up by P' points. Earth escape trajectories defined on $\mathcal{E}_{SE}^{-1}$, $\mathcal{E}_{SE}$ are taken into account, as the latter intersects a special subset leading to orbits at the Moon (see Fig. 4(b), where $\mathcal{E}_{SE}$ is reported).

It is worth noticing that the parking orbit is defined at a lower energy level than orbits on $\mathcal{E}_{SE}^{-1}$, therefore the instantaneous velocity change Δv_E is required to place the translunar trajectory on $F(C_{SE}) \cap \mathcal{E}_{SE}^{-1}$. In practice, this maneuver is provided by the launch vehicle once the spacecraft is on the Earth parking orbit. A mission profile including this parking orbit is in fact consistent with major architecture requirements, as summarized in.[15]

The design of the SE phase is reduced in this way to the determination of the two sets $\mathcal{E}_{SE}^{-1}$, $\mathcal{E}_{SE}$, and to the computation of Δv_E. This first phase of the transfer is constructed using Eqs. (1). The SE trajectory does not make use of low-thrust propulsion, and the phase space structure of the ballistic PCRTBP is exploited.

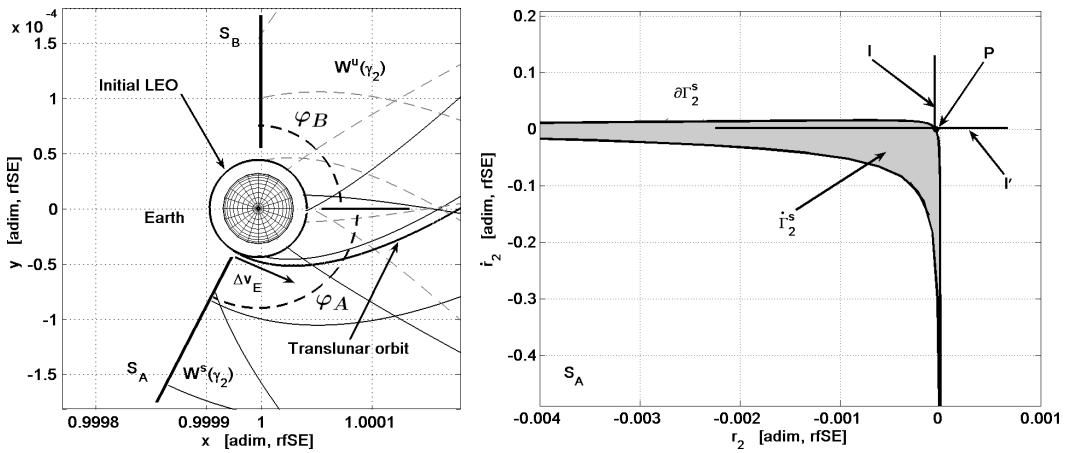

(a) Initial transfer condition.

(b) $\partial\,\Gamma_2^s$, $\dot{\Gamma}_2^s$, l, l' sets, and point $P = l \cap l'$.

Figure 2: Earth escape trajectory performed with a tangential Δv_E maneuver and its associated section point P.

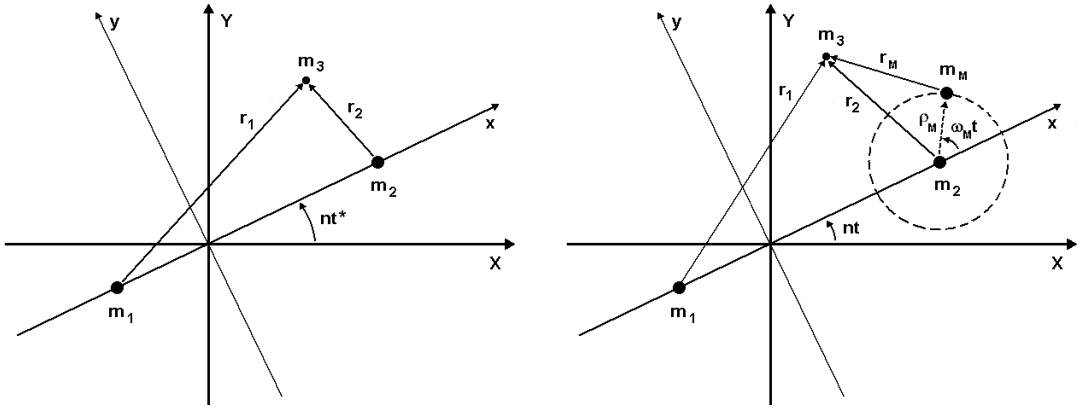

(a) Classic circular planar restricted three-body problem.

(b) Moon-perturbed Sun–Earth RTBP.

Figure 3: Mathematical models to described the physics of the problem.

3.1. The Moon-Perturbed Sun-Earth Restricted Three-Body Problem

When the gravitational attraction of the Moon is taken into account, Eqs. (1) are augmented with the dynamics of the Moon; this leads to formulate the bicircular restricted four-body problem, BRFBP (see Fig. 3(b)). The dynamical system moves from the fourth order to the fifth one. Some assumptions are taken into account, recalling that the orbits of the primaries show low eccentricity values (≈ 0.01, ≈ 0.04), and the Moon inclination with respect to the ecliptic plane is little ($\approx 5\,\text{deg}$): (i) the Sun and the Earth are revolving in circular orbits around their center of mass; (ii) the Earth–Moon barycenter is moving in a circular orbit around the center of mass of the Sun–Earth–Moon system.

Assuming all the hypothesis written above, the planar equations of motion are:

$$\ddot{x} - 2\dot{y} = \frac{\partial \Omega_M}{\partial x}, \qquad \ddot{y} + 2\dot{x} = \frac{\partial \Omega_M}{\partial y}, \qquad \dot{\theta} = \omega_M \tag{8}$$

where the subscripts denote the partial derivative of the auxiliary function

$$\Omega_M(x, y, \theta) = \Omega(x, y, \mu_{SE}) + \frac{m_M}{r_M} - \frac{m_M}{\rho_M^2}\,(x\cos\theta + y\sin\theta). \tag{9}$$

The quantity $\Omega(x, y, \mu_{SE})$ stands for the classic RTBP potential expressed by Eq. (2), while the remaining part represents the gravitational perturbation of the Moon.

The dimensionless physical constants introduced to describe the Moon influence are in agreement with those of the SE model. Thus, the distance between the Moon and the Earth is $\rho_M = 2.5721 \times 10^{-3}$, the mass of the Moon is $m_M = 3.6942 \times 10^{-8}$, and its angular velocity with respect to the SE rotating frame is $\omega_M = 1.2367 \times 10^1$. The location of the Moon is therefore at $(1 - \mu_{SE} + \rho_M \cos\theta, \rho_M \sin\theta)$, such that:

$$r_M^2 = (x - 1 + \mu_{SE} - \rho_M \cos\theta)^2 + (y - \rho_M \sin\theta)^2. \tag{10}$$

According to the differential Eqs. (8), the system does not admit the existence of any libration point or integral of motion. Anyway, as the Moon can be considered as a small perturbation of the Sun–Earth model, a qualitative global analysis about the motion of the spacecraft is proposed, assuming the restricted four-body model as a perturbation of the invariant objects of the classic RTBP. If the points belonging to the escape set $\mathcal{E}_{SE}$ are backwards integrated under the dynamics associated with Eqs. (8), the topology of their trajectories in the configuration space is only slightly and negligible different. The main variations appear associated with the pre-image set $\mathcal{E}_{SE}^{-1}$. If the trajectories pass nearby the Moon, the points $P' \in S_A$ show almost the same phase-space coordinates $(r_2, \dot{r}_2)$ as before, while the tangential velocity reduces significantly, with respect to the classic Sun–Earth RTBP computation. In details, when a lunar flyby is explicitly taken into account while designing the Earth escape stage, the difference between the energy level of the parking orbit at a height $h_E = 167\,\text{km}$ and the one of the orbits on $\mathcal{E}_{SE}^{-1}$ is lowered. This means that a reduced instantaneous velocity change Δv_E is now required to place the translunar trajectory on $F(C_{SE}) \cap \mathcal{E}_{SE}^{-1}$.

4. Low-Thrust Propulsion and Attainable Sets

Once the initial transfer stage is defined, the final one that leads to the Moon is required. The core of the formulation is based on a perturbed version of the classic RTBP. The perturbation is the low-thrust propulsion, and when its driving parameters are wisely tuned, different types of transfer arcs, as well as several final conditions at the Moon, can be investigated.

To model the *controlled* motion of m_3 under both the gravitational attractions of m_1, m_2, and the low-thrust propulsion, the following differential equations are considered:

$$\ddot{x} - 2\dot{y} = \frac{\partial\Omega}{\partial x} + \frac{T_x}{m}, \quad \ddot{y} + 2\dot{x} = \frac{\partial\Omega}{\partial y} + \frac{T_y}{m}, \quad \dot{m} = -\frac{T}{I_{sp}\, g_0}, \tag{11}$$

where $T = \sqrt{T_x^2 + T_y^2}$ is the thrust magnitude, I_{sp} the specific impulse of the engine and g_0 the gravitational acceleration at sea level. The ballistic motion (Eqs. (1)) is represented

by a fourth-order system, while the controlled motion (Eqs. (11)) is described by a fifth-order system of differential equations. Continuous variations of the spacecraft mass, m, are taken into account when low-thrust propulsion is considered. This causes a singularity arising when $m \to 0$, beside the well-known singularities given by impacts of m_3 with m_1 or m_2.

The thrust law $\mathbf{T}(t) = \{T_x(t), T_y(t)\}^\top$, $t \in [t_i, t_f]$, in Eqs. (11) is not given, but rather in this approach it represents an unknown that is found when the optimal control problem is solved (t_i and t_f are the initial and final times, respectively). It is determined such that a certain state is targeted and, at the same time, a certain objective function is minimized. However, in order to build first guess solutions, at this stage the profile of $\mathbf{T}$ over time is described. In particular, using tangential thrust, attainable sets can be defined in the same fashion as reachable sets are defined in.[8]

Let $\mathbf{y}_i$ be a vector representing a generic initial state, i.e., $\mathbf{y}_i = \{x_i, y_i, \dot{x}_i, \dot{y}_i, m_i\}^\top$, and let $\phi_{\mathbf{T}(\tau)}(\mathbf{y}_i, t_i; t)$ be the flow of system of Eqs. (11) at time t, starting from $(\mathbf{y}_i, t_i)$ and considering the thrust profile $\mathbf{T}(\tau)$, $\tau \in [t_i, t]$. The latter has to be taken within proper bounds that are typically given by technological constraints. This condition usually reads $T(t) \leq T_{max}$, where T_{max} is the maximum available thrust magnitude. With this notation, it is possible to define the generic point of a tangential low-thrust trajectory through

$$\mathbf{y}(t) = \phi_{\overline{\mathbf{T}}}(\mathbf{y}_i, t_i; t), \tag{12}$$

where $\overline{\mathbf{T}} = \overline{T}\,(\mathbf{v}/v)$, $v = \sqrt{\dot{x}^2 + \dot{y}^2}$, $\mathbf{v} = \{\dot{x}, \dot{y}\}^\top$. Eq. (12) represents the flow of the differential system governed by Eqs. (11), when constant tangential thrust of magnitude $\overline{T}$ is considered. With given $\overline{T}$, tangential thrust maximizes the variation of Jacobi energy, which is the only property that has to be dealt with when designing trajectories in the RTBP. (In,[16] a comparison between tangential thrust in either rotating or inertial frame is proposed). The low-thrust orbit, at time t, can be expressed as

$$\gamma_{\overline{\mathbf{T}}}(\mathbf{y}_i, t) = \{\phi_{\overline{\mathbf{T}}}(\mathbf{y}_i, t_i; \tau) | \tau < t\}, \tag{13}$$

where the dependence on the initial state $\mathbf{y}_i$ is kept. The attainable set, at time t, can be defined as

$$\mathcal{A}_{\overline{\mathbf{T}}}(t) = \bigcup_{\mathbf{y}_i \in \mathcal{Y}} \gamma_{\overline{\mathbf{T}}}(\mathbf{y}_i, t), \tag{14}$$

where $\mathcal{Y}$ is a domain of admissible initial conditions. Attainable set in equation Eq. (14) is associated with a generic $\mathcal{Y}$; this set can be suitably defined for the three different types of transfers at hand. Thanks to the definition of $\mathcal{A}_{\overline{\mathbf{T}}}(t)$, low-thrust propulsion can be incorporated in a three-body frame, using the same methodology developed for the invariant manifolds.[3] More specifically, invariant manifolds are replaced by attainable sets which are manipulated (i.e., intersected) to find a transfer point on a suitable surface of section. The idea is to mimic the role that invariant manifolds have in trajectory design with the use of attainable sets. This approach can be adapted to design either two-impulse transfers as well as low-thrust transfers to the Moon.

4.1. Moon Ballistic Capture Stage

In analogy with what described for the Earth escape stage in section 3, by fixing a suitable value of the Jacobi constant in the EM model, C_{EM}, a unique Lyapunov orbit about both L_1 and L_2, named λ_1 and λ_2, respectively, can be defined. Restricting the energy to $C_{EM} \ll C_{2-EM}$ (where C_{2-EM} is the Jacobi constant of L_2 in the EM model), both λ_1 and λ_2 exist, and the Hill's regions are opened at both L_1 and L_2. In order to reach the final orbit about the Moon from the exterior, a capture via L_2 is considered (see Fig. 4(a)). This means that the Moon ballistic capture stage is constructed by exploiting the dynamics around L_2. The stable manifold associated with λ_2, $W^s(\lambda_2)$, is computed starting from λ_2 and integrating backward until a certain surface of section is reached. Section S_C, making an angle φ_C (counterclockwise) with the x-axis and passing through the Earth, is considered to cut $W^s(\lambda_2)$ ($\varphi_C = \pi/2$ in Fig. 4(a)). The corresponding section curve, $\partial\,\Lambda_2^s$ (computed on the $(r_1, \dot{r}_1)$-plane in the EM model), is diffeomorphic to a circle. The set $\mathcal{K}_{EM} = \dot{\Lambda}_2^s$ is defined, where $\dot{\Lambda}_2^s \in S_C$ is the set of points inside $\partial\,\Lambda_2^s$, set that leads to the Moon capture.

The set $\mathcal{K}_{EM}$ is defined on section S_C in the EM model. However, it is possible to represent $\mathcal{K}_{EM}$ on S_B defined in the SE model through the transformation $\tilde{\mathcal{K}}_{EM} = \mathcal{M}(\mathcal{K}_{EM})$. The operator $\mathcal{M}$ maps states on S_C (EM model) to states on S_B (SE model), provided the two angles φ_C, φ_B. The same conversion is also applied to $\partial\,\Lambda_2^s$, in order to obtain $\partial\,\tilde{\Lambda}_2^s = \mathcal{M}(\partial\,\Lambda_2^s)$ on section S_B from section S_C. This transformation is basically made up of a rotation and a scaling of the variables in proper units (see Fig. 4(b) where $\tilde{\mathcal{K}}_{EM}$ and $\partial\,\tilde{\Lambda}_2^s$ are reported).

Considering only section S_B, it is possible to define the ballistic low energy Earth–Moon transfers as the orbits belonging to the set $\mathcal{E}_{SE} \cap \tilde{\mathcal{K}}_{EM}$. The sets $\mathcal{E}_{SE}$ and $\tilde{\mathcal{K}}_{EM}$ are characterized by different values of the Jacobi constant, C_{SE} and C_{EM}, respectively. In addition, any point in $\tilde{\mathcal{K}}_{EM}$ has a different value of Jacobi constant as $\mathcal{M}$ is not energy preserving. Thus, in order to join together orbits on $\mathcal{E}_{SE}$ and orbits on $\tilde{\mathcal{K}}_{EM}$, an impulsive maneuver at the patching point may be required.

This approach is the one known in literature to design Earth–Moon low energy transfers with impulsive maneuvers.[3] Indeed, another impulsive maneuver, besides the one performed at the patching point, is necessary upon Moon arrival to place the spacecraft into a stable orbit around the Moon. This approach is based on either Eqs. (1) or Eqs. (11) with $T = 0$, and allows to define low energy transfers like those described in.[1,2,4]

Two-impulse transfers to the Moon are defined as follows. The spacecraft is assumed to be initially on a parking orbit about the Earth with given eccentricity, e, and perigee/apogee altitude, h_p/h_a. The argument of perigee, ω_E, of this orbit is not fixed. The transfer begins when the spacecraft is at the perigee of this orbit. An impulsive maneuver, carried out by the launch vehicle, places the spacecraft onto a translunar trajectory; from this point on, the spacecraft flies ballistically under the RTBP dynamics until it reaches the Moon neighborhood. Then, a second impulsive maneuver is required to insert the spacecraft into a stable orbit around the Moon. This orbit has moderate eccentricity, e, and periapsis/apoapsis altitude h_p/h_a, prescribed by the mission require-

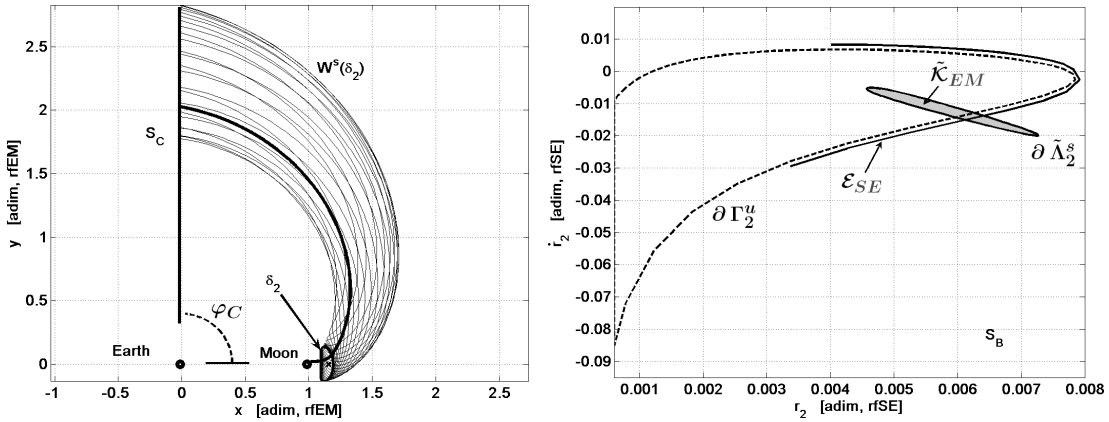

(a) $W^s(\lambda_2)$. (b) $\mathcal{E}_{SE}$ and $\tilde{\mathcal{K}}_{EM}$ sets.

Figure 4: Stable manifold $W^s(\lambda_2)$ and its section curve $\partial\,\tilde{\Lambda}^s_2$. The latter is used to define the set of orbits that lead to Moon capture $\tilde{\mathcal{K}}_{EM}$. In Fig. 4(a), the bold line stands for a sample Moon capture trajectory.

ments. The transfer terminates when the spacecraft is at the periapsis of this orbit. While both e and r_p/r_a are given, the orientation, i.e., the argument of periapsis, ω_M, of the final orbit around the Moon is not fixed.

The global transfer is designed recalling the coupled RTBPs approximation. The initial orbit is a trajectory belonging to the set $\mathcal{E}_{SE}$, whereas the second part is defined using a suitable attainable set in the EM model, according to the formalism introduced in section 4, Eq. (14). As this set constitutes the second part of the trajectory, it is made up by ballistic orbits that are integrated backward, i.e., considering the thrust magnitude $T = 0$. More specifically, as both eccentricity and apsidal altitude are prescribed, the final state of the transfers (i.e., the periapsis point of the orbit about the Moon) is function of the argument of periapsis and of the final tangential Δv_M impulsive maneuver required to place the spacecraft into a stable lunar orbit, i.e., $\mathbf{y}_f = \mathbf{y}_f(\omega_M, \Delta v_M)$, see Fig. 5(a).

According to this approach, the domain of admissible final states becomes

$$\mathcal{Y}^M = \{\mathbf{y}_f(\omega_M, \Delta v_M) | \omega_M \in [0, 2\pi], \Delta v_M \in [0, +\infty]\}, \tag{15}$$

and the attainable set, for some $t \geq 0$ (i.e., $-t$ is a backward integration), containing ballistic capture trajectories with impulsive stabilization is

$$\mathcal{A}^M_{\mathbf{B}}(-t) = \bigcup_{\mathbf{y}_f \in \mathcal{Y}^M} \gamma_{\mathbf{B}}(\mathbf{y}_f(\omega_M, \Delta v_M), -t). \tag{16}$$

Each generic Moon capture orbit written in Eq. (16), at time $-t$, can be expressed as

$$\gamma_{\mathbf{B}}(\mathbf{y}_f, -t) = \{\phi_{\mathbf{B}}(\mathbf{y}_f, t_f; -\tau) | -\tau > -t\}, \tag{17}$$

where $\mathbf{B} = T\,(\mathbf{v}/v)$, $v = \sqrt{\dot{x}^2 + \dot{y}^2}$, $\mathbf{v} = \{\dot{x}, \dot{y}\}^\top$, and assuming $T = 0$. Since the first part of the transfer is defined on $\mathcal{E}_{SE}$, the transfer points, if any, that generate two-impulse

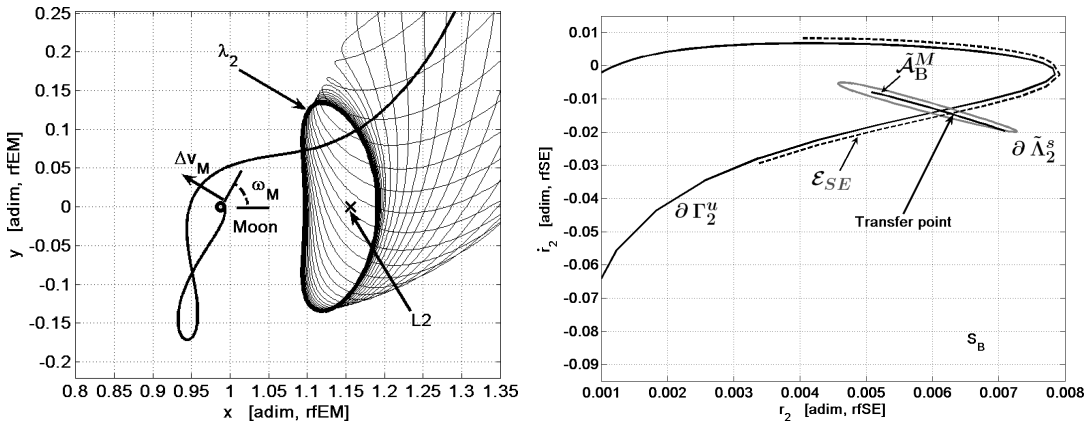

(a) Sample impulsive capture trajectory.

(b) $\mathcal{E}_{SE}$ and $\tilde{\mathcal{A}}^M_{\mathbf{B}}(-t)$ sets.

Figure 5: The first guess impulsive capture solution as the transfer point $\mathcal{B}^M_{-t} = \mathcal{E}_{SE} \cap \tilde{\mathcal{A}}^M_{\mathbf{B}}(-t)$, the latter reported on section S_B in Fig. 5(b).

transfers are contained in the set

$$\mathcal{B}^M_{-t} = \mathcal{E}_{SE} \cap \tilde{\mathcal{A}}^M_{\mathbf{B}}(-t). \tag{18}$$

Once again, the transformation $\mathcal{M}$ is required to map $\mathcal{A}^M_{\mathbf{B}}(-t)$, computed in the EM model, into $\tilde{\mathcal{A}}^M_{\mathbf{B}}(-t)$, defined in the SE model, see Fig. 5(b). At this stage, first guesses are defined, and therefore states with small, tolerable mismatches can be admitted in $\mathcal{B}^M_{-t}$; this tolerance is chosen such that the discontinuities can be easily spread in the subsequent optimization step.

4.2. Moon Low-Thrust Capture Stage

Dealing with the design of low-energy, low-thrust transfers to the Moon, the initial and final conditions at the Earth and the Moon, respectively, are assumed in the same way as described in section 4.1 for the two-impulse trajectories. Actually, this case differs from the previous one in the fact that low-thrust contribution is explicitly taken into account. As part of the coupled RTBPs approximation, in connection with the Earth escape stage, the continuously propelled capture stage is used with the low-thrust term preliminary acting only in the EM model. Thus, the initial orbit is a trajectory belonging to the set $\mathcal{E}_{SE}$, whereas the second part is defined using a suitable attainable set. This set constitutes the second part of the trajectory and it is made up by tangential low-thrust orbits that are integrated backward. More specifically, as both eccentricity and apsidal altitude are prescribed, the final state of the transfers (i.e., the periapsis point of the orbit about the Moon) is function of the argument of periapsis, $\mathbf{y}_f = \mathbf{y}_f(\omega_M)$, as shown in Fig. 6(a). The domain of admissible final states therefore is

$$\mathcal{Y}^M = \{\mathbf{y}_f(\omega_M) | \omega_M \in [0, 2\pi]\}, \tag{19}$$

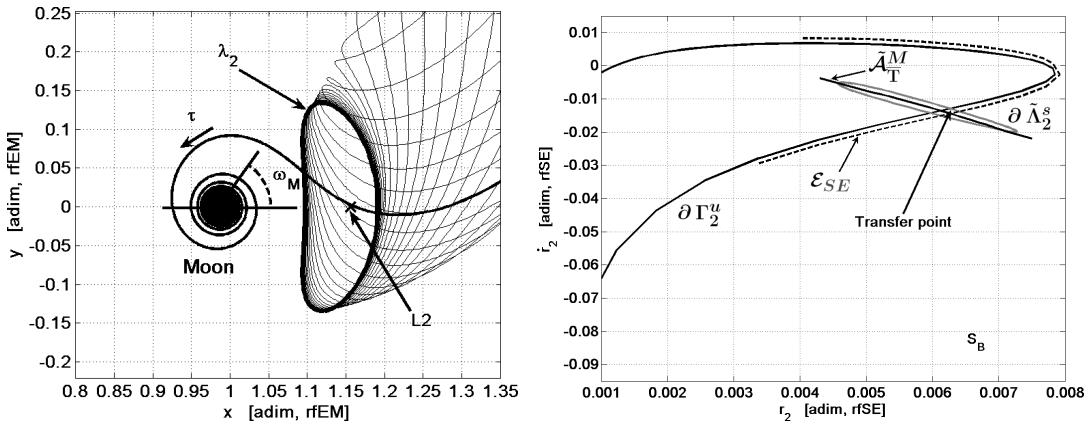

(a) Sample low-thrust capture trajectory.

(b) $\mathcal{E}_{SE}$ and $\tilde{\mathcal{A}}^M_{\mathbf{T}}(-t)$ sets.

Figure 6: The first guess low-thrust capture solution as the transfer point $\mathcal{T}^M_{-t} = \mathcal{E}_{SE} \cap \tilde{\mathcal{A}}^M_{\mathbf{T}}(-t)$, the latter reported on section S_B in Fig. 6(b).

and the attainable set, for some $t \geq 0$ ($-t$ is a backward integration), containing low-thrust, ballistic capture trajectories is

$$\mathcal{A}^M_{\mathbf{T}}(-t) = \bigcup_{\mathbf{y}_f \in \mathcal{Y}^M} \gamma_{\mathbf{T}}(\mathbf{y}_f(\omega_M), -t). \tag{20}$$

Since the first part of the transfer is defined on $\mathcal{E}_{SE}$, the transfer points, if any, that generate low-energy, low-thrust transfers are contained in the set

$$\mathcal{T}^M_{-t} = \mathcal{E}_{SE} \cap \tilde{\mathcal{A}}^M_{\mathbf{T}}(-t). \tag{21}$$

The transformation $\mathcal{M}$ is required to map $\mathcal{A}^M_{\mathbf{T}}(-t)$, computed in the EM model, into $\tilde{\mathcal{A}}^M_{\mathbf{T}}(-t)$, defined in the SE model, as shown in Fig. 6(b). It is worth mentioning that first guess solutions are being generated in this step. These preliminary solutions have to be later optimized in a four-body context. Again, small discontinuities can be tolerated when looking for the transfer point. This means that it is possible to intersect two states such that $\|\mathbf{y}_A - \mathbf{y}_E\| \leq \varepsilon$, where $\mathbf{y}_E \in \mathcal{E}_{SE}$, $\mathbf{y}_A \in \tilde{\mathcal{A}}^M_{\mathbf{T}}(-t)$, and ε is a prescribed tolerance. The greater ε is, the higher number of first guess solutions is found; however, ε should be kept sufficiently small to permit the convergence of the subsequent optimization step.

5. Trajectory Optimization

Once feasible and efficient first guess solutions are achieved, combining attainable sets with Earth-escape sets, an optimal control problem is stated in the BRFBP framework. The model used to take into account the low-thrust propulsion and the gravitational attractions of all the celestial bodies involved in the design process (the Sun, the Earth, and the Moon) is

$$\ddot{x} - 2\dot{y} = \frac{\partial \Omega_S}{\partial x} + \frac{T_x}{m}, \quad \ddot{y} + 2\dot{x} = \frac{\partial \Omega_S}{\partial y} + \frac{T_y}{m}, \quad \dot{\theta} = \omega_S, \quad \dot{m} = -\frac{T}{I_{sp}\, g_0}. \tag{22}$$

This is a modified version of the classic bicircular four-body problem[17] (see Fig. 7(a)) and, in principle, incorporates the perturbation of the Sun into the Earth–Moon RTBP described by Eqs. (1). The four-body potential Ω_S reads

$$\Omega_S(x, y, \theta) = \Omega(x, y, \mu_{EM}) + \frac{m_S}{r_S} - \frac{m_S}{\rho_S^2}(x\cos\theta + y\sin\theta). \tag{23}$$

The dimensionless physical constants introduced to describe the Sun perturbation are in agreement with those of the EM model. Thus, the distance between the Sun and the Earth–Moon barycenter is $\rho_S = 3.8878 \times 10^2$, the mass of the Sun is $m_S = 3.2890 \times 10^5$, and its angular velocity with respect to the EM rotating frame is $\omega_S = -9.2518\times10^{-1}$. The Sun is located at $(\rho_S\cos\theta, \rho_S\sin\theta)$, and therefore the Sun-spacecraft distance is calculated as

$$r_S^2 = (x - \rho_S\cos\theta)^2 + (y - \rho_S\sin\theta)^2. \tag{24}$$

This low-thrust version of the BRFBP is represented by the sixth-order system of differential Eqs. (22).

According to the formalism proposed in,[18] the controlled BRFBP described by Eqs. (22) is written in the first-order form

$$\begin{aligned}
\dot{x} &= v_x \\
\dot{y} &= v_y \\
\dot{v}_x &= 2v_y + \Omega_{Sx} + T_x/m \\
\dot{v}_y &= -2v_x + \Omega_{Sy} + T_y/m \\
\dot{\theta} &= \omega_S \\
\dot{m} &= -T/(I_{sp}\, g_0),
\end{aligned} \tag{25}$$

with $v_x = \dot{x}$ and $v_y = \dot{y}$. In a compact explicit form, system (Eqs. (25)) reads

$$\dot{\mathbf{y}} = \mathbf{f}[\mathbf{y}(t), \mathbf{T}(t), \mathbf{p}, t], \tag{26}$$

where $\mathbf{f}$ stands for the vector field, $\mathbf{T} = \{T_x, T_y\}^\top$ is the thrust vector, and $\mathbf{y} = \{x, y, v_x, v_y, \theta, m\}^\top$ is the state vector. In addition, the dynamics is also allowed to incorporate some constant parameters $\mathbf{p}$ useful for the definition of the optimal control problem. The aim is finding, according to the standard optimal control theory, the guidance law $\mathbf{T} = \mathbf{T}(t)$, $t \in [t_i, t_f]$, that minimizes a prescribed scalar performance index or objective function

$$J = J(\mathbf{y}, \mathbf{T}, \mathbf{p}, t), \tag{27}$$

while satisfying certain mission constraints. These constraints are represented by the two boundary conditions, defined at the endpoints of the optimal control problem, and by the inequality conditions, defined along the whole arc. These last quantities are derived specifically for each of the three types of mission to Moon that are investigated.

The optimal control problem (OCP) is then transcribed into a nonlinear programming (NLP) problem using a direct approach. This method, although suboptimal, generally

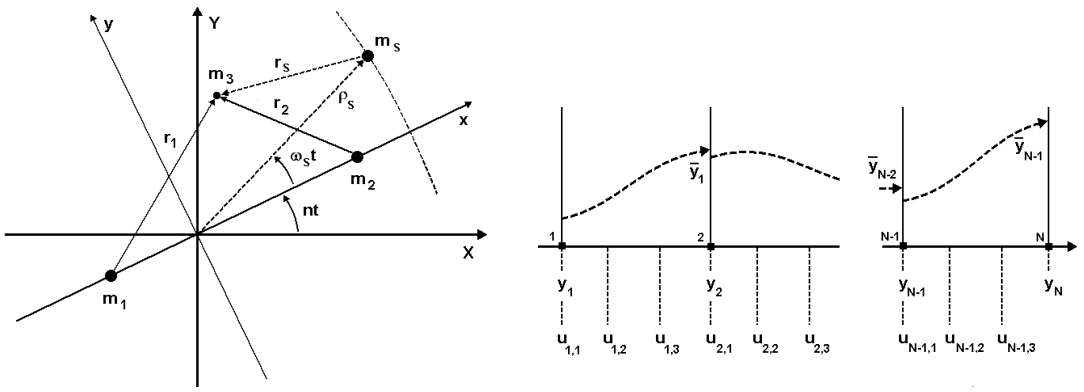

(a) Sun-perturbed Earth–Moon RTBP.

(b) Direct multiple shooting scheme.

Figure 7: Optimization process, dynamical model and integration scheme.

shows robustness and versatility, and does not require explicit derivation of the necessary conditions of optimality. Moreover, direct approaches offer higher computational efficiency and are less sensitive to variation of the first guess solutions.[18] Numerically, a multiple shooting scheme is implemented. With this strategy the BRFBP dynamics presented by Eqs. (25) is forward integrated within $N-1$ intervals (in which $[t_i,\, t_f]$ is uniformly split); i.e., the time domain is divided into $t_i = t_1 < \cdots < t_N = t_f$, and the solution is discretized over the N grid nodes (see Fig. 7(b)). The continuity of position, velocity and mass is imposed at their ends,[19] in the form of defects $\boldsymbol{\eta}_j = \bar{\mathbf{v}}_j - \mathbf{v}_{j+1} = 0$, for $j = 1, \ldots, N-1$. The quantity $\bar{\mathbf{v}}_j$ stands for the result of the integration, i.e., $\bar{\mathbf{v}}_j = \boldsymbol{\phi}(\mathbf{v}_j, \mathbf{p}, t)$, $t_j \leq\ t_{j+1}$, and is made up of state variables and control variables ($\mathbf{v}_j = \{\mathbf{y}_j, \mathbf{T}_{j,k}\}^\top$, for $k = 1, \ldots, M-1$). The control law $\mathbf{T}(t)$ is described within each interval by means of cubic spline functions. The algorithm computes the value of the control at mesh points, satisfying both boundary and path constraints, and minimizing the performance index.

Dynamics described by Eqs. (22) are highly nonlinear and, in general, lead to chaotic orbits. In order to find accurate optimal solutions without excessively increasing the computational burden, an adaptive nonuniform time grid has been implemented. Thus, when the trajectory is close to either the Earth or the Moon the grid is automatically refined, whereas in the intermediate phase, where a weak vector field governs the motion of the spacecraft, a coarse grid is used. The optimal solution found is assessed a posteriori by forward integrating the optimal initial condition with a $7^{\text{th}}/8^{\text{th}}$ order Runge–Kutta scheme, and by cubic interpolation of the discrete optimal control solution. Not only the low-thrust portion, but rather the whole transfer trajectory is discretized and optimized, so allowing the low-thrust to act also in regions preliminary made up by coast arcs.

5.1. Two-Impulse Problem Statement

As far as it concerns two-impulse, low energy transfers to the Moon, the dynamical system described by Eqs. (25) has zero thrust and the Earth–Moon transfer is made up by coast arcs.

According to the NLP problem recalled in section 5, the variable vector is

$$\mathbf{x} = \{(\mathbf{y}, \mathbf{B})_1, \ldots, (\mathbf{y}, \mathbf{B})_N, t_1, t_N\}^\top, \tag{28}$$

where $\mathbf{B} = \{0, 0\}^\top$, i.e., the thrust magnitude is $T = 0$ along the whole time domain of the transfer.

The initial conditions read:

$$\boldsymbol{\psi}_i(\mathbf{y}_1, t_1) := \begin{cases} (x_1 + \mu)^2 + y_1^2 - r_i^2 = 0 \\ (x_1 + \mu)(\dot{x}_1 - y_1) + y_1(\dot{y}_1 + x_1 + \mu) = 0, \end{cases} \tag{29}$$

which force the first $\mathbf{y}_1$ state of the transfer to belong to a circular orbit of radius $r_i = R_E + h_E$, where R_E and h_E stand for the Earth radius and the orbit altitude with respect to the Earth, respectively. In analogy, the final conditions at the Moon are:

$$\boldsymbol{\psi}_f(\mathbf{y}_N, t_N) := \begin{cases} (x_N - 1 + \mu)^2 + y_N^2 - r_f^2 = 0 \\ (x_N - 1 + \mu)(\dot{x}_N - y_N) + y_N(\dot{y}_N + x_N - 1 + \mu) = 0, \end{cases} \tag{30}$$

according to which, the final $\mathbf{y}_N$ state of the transfer is on a circular orbit of radius $r_f = R_M + h_M$, where R_M and h_M stand for the Moon radius and the orbit altitude with respect to the Moon, respectively. Conditions written in Eqs. (29) and Eqs. (30) mean that in the reference frame centered in the Earth and the Moon, respectively, the position and velocity vectors are orthogonal.[20] The nonlinear equality constraint vector, made up of the boundary conditions and the ones representing the dynamics, is therefore written as follows:

$$\mathbf{c}(\mathbf{x}) = \{\boldsymbol{\psi}_i, \boldsymbol{\eta}_1, \ldots, \boldsymbol{\eta}_{N-1}, \boldsymbol{\psi}_f\}^\top. \tag{31}$$

Moreover, aiming at avoiding the collision with the two primaries, the following inequality constraints are imposed:

$$\boldsymbol{\Psi}_j^c(\mathbf{y}_j) := \begin{cases} R_E^2 - (x_j + \mu)^2 - y_j^2 \leq 0 \\ R_M^2 - (x_j - 1 + \mu)^2 - y_j^2 \leq 0, \end{cases} \qquad j = 2, \ldots, N-1. \tag{32}$$

Finally, the flight time is searched to be positive, i.e.,

$$\boldsymbol{\Psi}^t = t_1 - t_N \leq 0. \tag{33}$$

The complete inequality constraint vector therefore reads:

$$\mathbf{g}(\mathbf{x}) = \{\boldsymbol{\Psi}_2^c, \ldots, \boldsymbol{\Psi}_{N-1}^c, \boldsymbol{\Psi}^t\}^\top. \tag{34}$$

As for the performance index to minimize, this is a scalar that represents the two velocity variations at endpoints of the transfer, $J(\mathbf{x}) = \Delta v_1 + \Delta v_N$, where

$$\Delta v_1 = \sqrt{(\dot{x}_1 - y_1)^2 + (\dot{y}_1 + x_1 + \mu)^2} - v_i, \tag{35}$$

assuming $v_i = \sqrt{(1-\mu)/r_i}$ the velocity along the initial circular parking orbit around the Earth, and

$$\Delta v_N = \sqrt{(\dot{x}_N - y_N)^2 + (\dot{y}_N + x_N - 1 + \mu)^2} - v_f, \tag{36}$$

assuming $v_f = \sqrt{(\mu)/r_f}$ the velocity along the final circular orbit around the Moon.

In summary, the NLP problem for the two-impulse transfers is formulated as follows:

$$\min_{\mathbf{x}} \quad J(\mathbf{x}) \qquad \text{subject to} \quad \begin{array}{l} \mathbf{c}(\mathbf{x}) = 0, \\ \mathbf{g}(\mathbf{x}) \leq 0. \end{array} \tag{37}$$

This problem is solved with $N = 40$ grid nodes, uniformly spaced (time interval about two days). Within each interval, the maximum and minimum time step is automatically chosen by the Runge–Kutta integrator.

5.2. Low-Thrust Problem Statement

Dealing with low-energy low-thrust transfers to the Moon, their design is performed by means of an initial impulsive TLI maneuver, followed by a ballistic arc closed by a low-thrust capture around the Moon.

According to the NLP problem recalled in section 5, the variable vector is

$$\mathbf{x} = \{(\mathbf{y}, \mathbf{T})_1, \ldots, (\mathbf{y}, \mathbf{T})_N, t_1, t_N\}^\top, \tag{38}$$

where, in this case, the thrust vector is properly $\mathbf{T} = (T_x, T_y)^\top$. Although the first guess control law is aligned with the synodic velocity of the spacecraft (tangential thrust of magnitude $\overline{T}$), the optimization process acts on all the variable of Eq. (38), and it is free to modify the control history, within the technological limits of the engine.

Then, the equality constraint vector, made up of initial and final conditions, together with the dynamics defect $\boldsymbol{\eta}$ satisfaction, is proposed in the same way as Eq. (31) of section 5.1. Dealing with the inequality constraints, beside the ones preventing the collision of the spacecraft with the two primaries and the one that represents the positive time evolution of the trajectory, a path constraint is added. This is introduced to model the saturation of the low-thrust engine. Thus, the inequality $T(t) \leq T_{max} = 0.5\,\mathrm{N}$, $t \in [t_i, t_f]$, is imposed along the whole transfer.

The optimal control step aims at finding the guidance law, $\mathbf{T}(t)$, $t \in [t_i, t_f]$, that minimizes the hybrid performance index

$$J = \rho \Delta v_1 + \int_{t_i}^{t_f} \frac{T(t)}{I_{sp}\, g_0}\, \mathrm{d}t; \tag{39}$$

the first part stands for the initial impulsive translunar insertion maneuver (provided by the launcher and recalling Eq. (35)) while the second contribution corresponds to the propellant mass, $m_p = m_i - m(t_f)$, needed to perform the transfer. The tuning parameter ρ is a weight quantity introduced to wisely balance the two contributions in the objective index computing. It is worth noticing that the optimization process is performed on the NLP variables described by Eq. (38), which are already dimensionless and easy to deal with

as they show the same order of magnitude. In order to eliminate possible discontinuities, arising when the intersection of the orbits is not exact, each first guess is first pre-processed to minimize

$$J = \frac{1}{2} \int_{t_i}^{t_f} \mathbf{u}^\top \mathbf{u} \, \mathrm{d}t, \tag{40}$$

with $\mathbf{u}(t) = \mathbf{T}(t)/m(t)$. The resulting solution is later used to minimize the objective function described by Eq. (39). Numerical experiments have shown that performing an intermediate step with objective function of Eq. (40) better enforces the satisfaction of boundary conditions and path constraints.[16] Finally, the NLP problem for the low-energy low-thrust transfers is formulated as proposed by Eq. (37) at the end of section 5.1.

This type of mission is solved with $N = 100$ grid nodes, not uniformly spaced. In particular, for the first part of the transfers, 40 grid nodes are used (time interval about two days). For the lunar descending phase, 60 additional grid nodes are used, in order to better follow the strong vector field (time interval about six hours). Moreover, within each interval, the maximum and minimum time step is automatically chosen by the Runge–Kutta integrator.

6. Optimized Transfer Solutions

In this section the transfer solutions arising from the optimization process are presented. In section 1 two families of trajectories are discussed, according to different types of propulsion system. In the following, the optimized transfers to LLOs are proposed in terms of some relevant performance parameters.

6.1. Trajectories to low orbits around the Moon

Optimal solutions are presented. These transfers start from a circular parking orbit at an altitude of $h_E = 167\,\mathrm{km}$ around the Earth, and end at circular orbit around the Moon, at an altitude of $h_M = 100\,\mathrm{km}$. The results are shown in Tab. 1 as follows: the first three solutions (i.e., sol.1, sol.2, sol.3) correspond to the low-energy low-thrust transfers, while solution sol.4 represents a two-impulse, low-energy transfer. Some reference impulsive transfers found in literature have also been reported;[1,21,22,20] all of them begin from the same LEO and arrive at the same LLO.

Tab. 1 is organized as follows: the second column Δv_i stands for the initial impulsive maneuver that inserts the spacecraft onto the translunar trajectory. For the solutions computed in this work, they are a direct output of the optimization process, described in section 5. The third column Δv_f represents the final impulsive maneuver that permits a stable permanent capture into a circular parking orbit around the Moon. This comes out from the optimization step for sol.4, it is not present for the low-thrust transfers whereas for the reference solutions this term takes into account all the impulsive maneuvers necessary to carry out the transfers except for Δv_i (i.e., for an Hohmann transfer only the second burn necessary to place the spacecraft into the final orbit about the Moon is considered; for a WSB transfer, this term has to take into account the possible mid-course maneuver

Table 1: Two-impulse transfers and low-energy low-thrust transfers to LLOs. A set of impulsive reference solutions found in literature is also reported. (Yag: two-impulse transfers,[20] WSB: weak stability boundary, BP: bi-parabolic, Hoh: Hohmann, BE: bi-elliptic;[1] L1: via L_1 transit orbits;[21] Min: theoretical minimum[22]).

Type	Δv_i [m/s]	Δv_f [m/s]	f_f [adim.]	f_t [adim.]	Δt [days]
sol.1	3211	–	0.061	0.683	271
sol.2	3203	–	0.050	0.681	145
sol.3	3169	–	0.046	0.675	103
sol.4	3143	650	0.198	0.724	88
Yag	3137	718	0.216	0.730	44
WSB	3161	677	0.206	0.729	90–120
BP	3232	721	0.217	0.739	∞
BE	3161	987	0.284	0.756	55–90
L1	3265	629	0.192	0.734	255
Hoh	3143	848	0.250	0.742	5
Min	3099	622	0.191	0.718	–

as well as the final maneuver needed to place the spacecraft into the final orbit about the Moon; similar arguments apply also to the bi-elliptic and bi-parabolic transfers).

Then, the fourth column f_f is a direct output (i.e., it is part of the performance index to minimize, divided by $m_{TLI} = 1000\,\mathrm{kg}$) only for the first three solutions, and stands for the propellant mass fraction required to perform the transfers, after the translunar insertion. As for the others, the value written in Tab. 1 is the propellant mass fraction associated with the impulsive Δv_f maneuver. This, through the rocket equation reads

$$f_f = \frac{m_p}{m_{TLI}} = 1 - \exp\left(-\frac{\Delta v_f}{I_{sp}^{ht}\, g_0}\right), \tag{41}$$

where $I_{sp}^{ht} = 300\,\mathrm{s}$ is assumed as the typical specific impulse related to high-thrust chemical engines. The fifth column f_t represents the overall mass fraction necessary to complete the Earth–Moon transfers. Even if for low-energy low-thrust solutions, according to the design of the Earth escape stage described in section 3, the initial Δv_i is given by the launch vehicle, for a sake of a fair comparison, the cost of this maneuver is considered, as written below:

$$f_t = \frac{m_p}{m_i} = \left[1 - \exp\left(-\frac{\Delta v_i}{I_{sp}^{ht}\, g_0}\right)\right] + \frac{1}{m_i}\int_{t_i}^{t_f} \frac{T(t)}{I_{sp}^{lt}\, g_0}\,\mathrm{d}t, \tag{42}$$

where $I_{sp}^{lt} = 3000\,\mathrm{s}$ is assumed as the specific impulse related to low-thrust electrical engines. Finally, the last column on the right stands for the transfer time. Dealing with

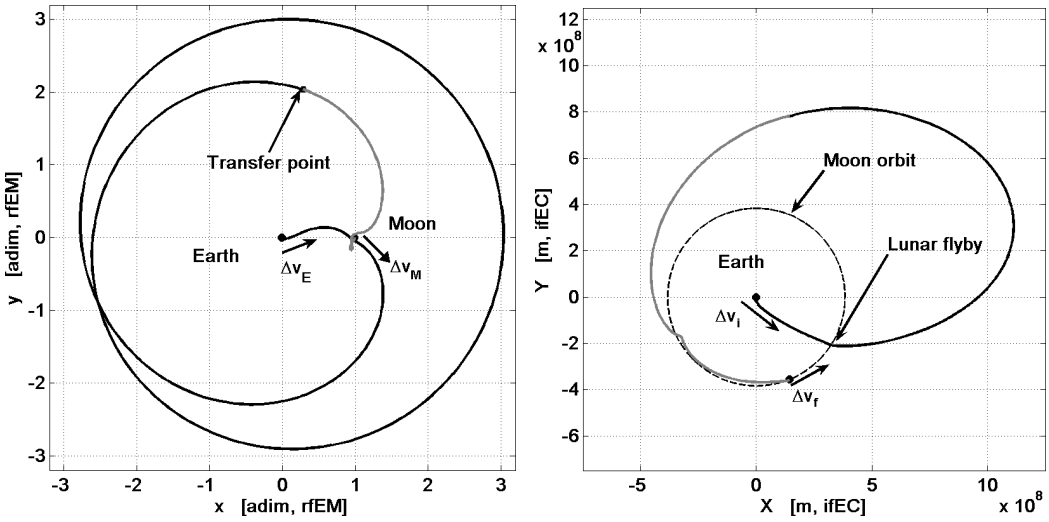

(a) First guess two-impulse trajectory, rotating EM reference frame.

(b) Optimized two-impulse trajectory, inertial geocentric reference frame.

Figure 8: Optimized two-impulse transfer to a low orbit around the Moon, corresponding to solution 4 in Tab. 1.

the last line, the minimum theoretical cost is computed via energetic considerations, and no associated solutions exist.

Few considerations about the first three low-energy, low-thrust transfers follow: moving from sol.1 to sol.3, the performances of the solutions improve, both in terms of Δv_i and Δt. This happens because the first guess trajectory related to sol.3 (in particular the Earth escape stage) is designed taking advantage explicitly of a lunar flyby at the beginning of the transfer, thanks to the Moon-perturbed Sun-Earth restricted three-body model. Moreover, the plane where Poincaré sections are considered and where the set $\mathcal{T}^M_{-t} = \mathcal{E}_{SE} \cap \tilde{\mathcal{A}}^M_{\mathbf{T}}(-t)$ is defined, is chosen tuning shrewdly φ_B and φ_C angles, in order to reduce the flight time.

In any case, sol.3, shown in Fig. 9, offers the lowest value of the overall mass consumption (see f_t). This happens for two reasons: firstly, the low-thrust, I^{lt}_{sp}, is one order of magnitude greater than I^{ht}_{sp}. Secondly, the first guess solutions exploit deeply the dynamics of the RTBPs where they are designed, and later of the Earth–Moon BRFBP where they are optimized. Moreover, these trajectories take explicitly advantage of the initial lunar flyby. The latter can be seen as an aid in the translunar orbit insertion, as it reduces the Δv_i required for that maneuver. The two-impulse trajectory corresponding to sol.4, shown in Fig. 8, acknowledges these remarks, as it shows the lowest global $\Delta v = 3793\,\mathrm{m/s}$ (with flight time $\Delta t = 88\,\mathrm{days}$). These considerations are in total accordance with what can be inferred from the rocket equation (see Eq. (42)): in order to reduce the total mass consumption, Δv has to decrease and I_{sp} has to increase. Finally, as far as it concerns the transfer times, the presented solutions turn out to be comparable with standard low energy transfers in terms of time of flight, although the latter are outperformed in terms of propellant mass.

Moreover, as for sol.3, in Fig. 9(c) and in Fig. 9(d), the control history profile and the

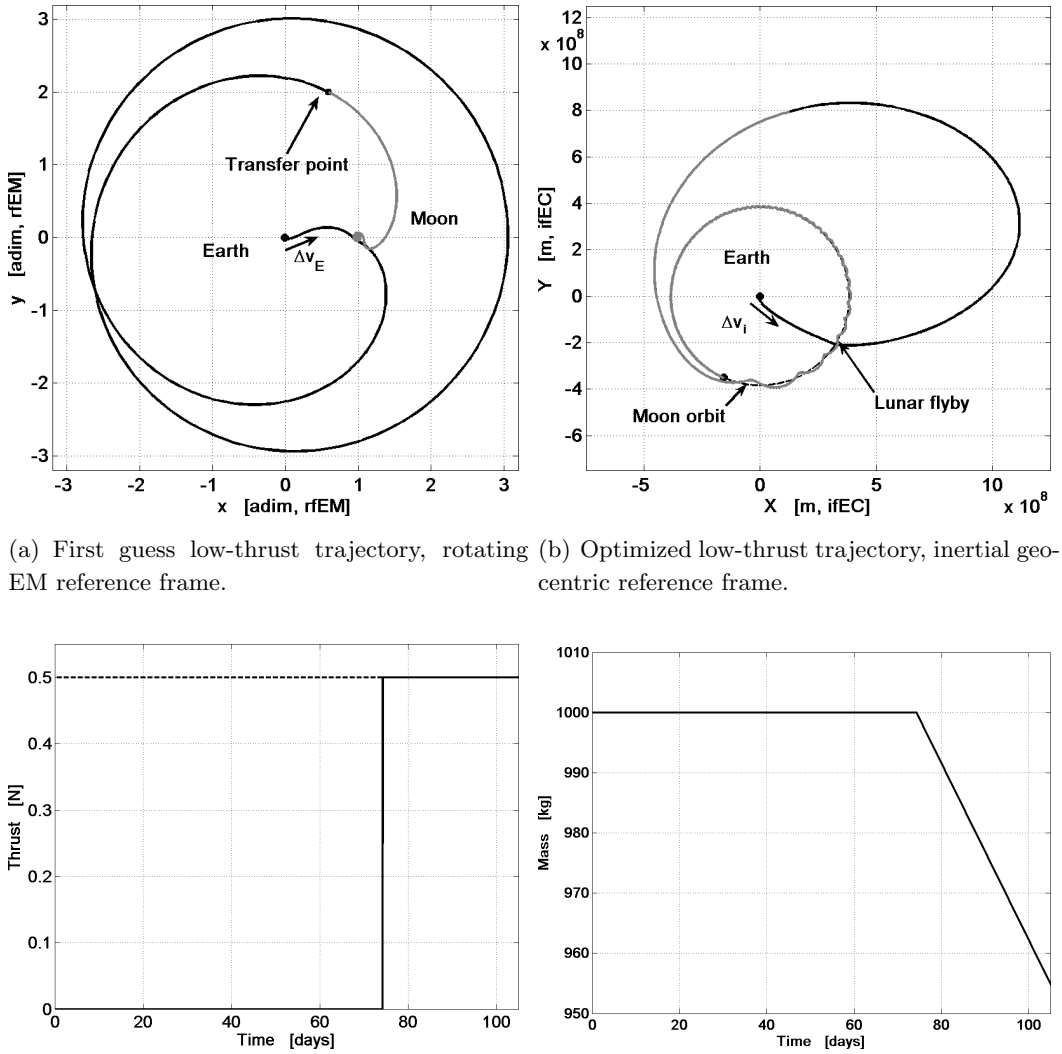

(a) First guess low-thrust trajectory, rotating EM reference frame.

(b) Optimized low-thrust trajectory, inertial geocentric reference frame.

(c) Control force magnitude.

(d) Mass consumption.

Figure 9: Optimized low-energy low-thrust transfer to a low orbit around the Moon, corresponding to solution 3 in Tab. 1.

mass consumption are reported, respectively. It is evident that the thrust magnitude is always below the saturation limit (dashed line in Fig. 9(c)). Furthermore, when the engine is on duty (at the end of the trajectory in order to perform the low-thrust capture around the Moon), it works at the maximum level: the control profile is optimal as it recalls an *on-off* structure.

7. Conclusions

In this paper two different technique to design Earth-to-Moon transfers have been investigated. Two-impulse, low-energy transfers as well as low-energy, low-thrust transfers have been formulated and optimized. The optimized solutions reveal to be efficient, both in terms of propellant mass consumption and flight time. With respect to the previous

work of the same authors,[11] the design methodology reveals to be more formal and easier to apply to different applicative scenarios. Improvements with respect to our previous studies have been obtained thanks to the exploitation of lunar flybys.

References

[1] E.A. Belbruno and J.K. Miller. Sun-Perturbed Earth-to-Moon Transfers with Ballistic Capture. *Journal of Guidance Control and Dynamics*, 16:770–775, 1993.

[2] E.A. Belbruno. *The Dynamical Mechanism of Ballistic Lunar Capture Transfers in the Four-Body Problem from the Perspective of Invariant Manifolds and Hill'S Regions*. Barcelona, Spain, 1994.

[3] W. Koon, M. Lo, J. Marsden, and S. Ross. Low Energy Transfer to the Moon. *Celestial Mechanics and Dynamical Astronomy*, 81:63–73, 2001.

[4] G. Gómez, W. Koon, M. Lo, J. Marsden, J. Masdemont, and S. Ross. Invariant Manifolds, the Spatial Three-Body Problem, and Space Mission Design. *Advances of the Astronautical Sciences*, 109:3–22, 2001.

[5] J.S. Parker and M.W. Lo. Shoot The Moon 3D. *Advances in the Astronautical Sciences*, 123, 2006.

[6] E.A. Belbruno. Lunar Capture Orbits, a Method of Constructing Earth Moon Trajectories and the Lunar Gas Mission. In *AIAA, DGLR, and JSASS, International Electric Propulsion Conference, 19th, Colorado Springs, CO, May 11-13, 1987. 10 p.*, 1987.

[7] J. Schoenmaekers, D. Horas, and J.A. Pulido. SMART-1: With Solar Electric Propulsion to the Moon. In *Proceedings of the 16th International Symposium on Space Flight Dynamics*, 2007.

[8] M. Dellnitz, O. Junge, M. Post, and B. Thiere. On Target for Venus: Set Oriented Computation of Energy Efficient Low Thrust Trajectories. *Celestial Mechanics and Dynamical Astronomy*, 95:357–370, 2006.

[9] G. Mingotti and F. Topputo, F. Bernelli-Zazzera. Combined Optimal Low-Thrust and Stable-Manifold Trajectories to the Earth–Moon Halo Orbits. In *American Institute of Physics Conference Proceedings*, volume 886, pages 100–110, 2007.

[10] MT Ozimek, DJ Grebow, and KC Howell. Design of Solar Sail Trajectories with Applications to Lunar South Pole Coverage. *Journal of guidance, control, and dynamics*, 32(6), 2009.

[11] G. Mingotti, F. Topputo, and F. Bernelli-Zazzera. Low-energy, low-thrust transfers to the Moon. *Celestial Mechanics and Dynamical Astronomy*, 105(1-3):61–74, 2009.

[12] V. Szebehely. *Theory of Orbits: the Restricted Problem of Three Bodies*. Academic Press New York, 1967.

[13] C. Conley. Low Energy Transit Orbits in the Restricted Three-Body Problem. *SIAM Journal of Applied Mathematics*, 16:732–746, 1968.

[14] J. Llibre, R. Martinez, and C. Simó. Transversality of the Invariant Manifolds associated to the Lyapunov Family of Periodic Orbits near L_2 in the Restricted Three-Body Problem. *Journal of Differential Equations*, 58:104–156, 1985.

[15] E. Perozzi and A. Di Salvo. Novel Spaceways for Reaching the Moon: an Assessment for Exploration. *Celestial Mechanics and Dynamical Astronomy*, 102:201–218, 2008.

[16] G. Mingotti, F. Topputo, and F. Bernelli-Zazzera. Numerical Methods to Design Low-Energy, Low-Thrust Sun-Perturbed Transfers to the Moon. In *Proceedings of 49th Israel Annual Conference on Aerospace Sciences, Tel Aviv–Haifa, Israel*, pages 1–14, 2009.

[17] C. Simó, G. Gómez, A. Jorba, and J. Masdemont. The Bicircular Model near the Triangular Libration Points of the RTBP. In *From Newton to Chaos*, pages 343–370, 1995.

[18] J.T. Betts. Survey of Numerical Methods for Trajectory Optimization. *Journal of Guidance control and dynamics*, 21(2):193–207, 1998.

[19] P.J. Enright and B.A. Conway. Discrete Approximations to Optimal Trajectories Using Direct Transcription and Nonlinear Programming. *Journal of Guidance Control and Dynamics*, 15:994–1002, 1992.

[20] K. Yagasaki. Sun-Perturbed Earth-to-Moon Transfers with Low Energy and Moderate Flight Time. *Celestial Mechanics and Dynamical Astronomy*, 90(3):197–212, 2004.

[21] F. Topputo, M. Vasile, and F. Bernelli-Zazzera. Earth-to-Moon Low Energy Transfers Targeting L1 Hyperbolic Transit Orbits. *Annals-New York Academy of Sciences*, 1065:55, 2005.

[22] T.H. Sweetser. An estimate of the global minimum DV needed for earth-moon transfer. In *Spaceflight mechanics 1991; Proceedings of the 1st AAS/AIAA Annual Spaceflight Mechanics Meeting, Houston, TX*, pages 111–120, 1991.